Published in "Europhysics Letters 88(3): 36004, 2009"
which should be cited to refer to this work.

X-ray reflectivity reveals equilibrium density profile of molecular liquid under nanometre confinement

E. Perret[1], K. Nygård[1], D. K. Satapathy[2], T. E. Balmer[3], O. Bunk[1], M. Heuberger[4] and J. F. van der Veen[1,3(a)]

[1] *Paul Scherrer Institut - 5232 Villigen PSI, Switzerland*
[2] *Université Fribourg - 1700 Fribourg, Switzerland*
[3] *ETH Zürich - 8093 Zürich, Switzerland*
[4] *EMPA - 9014 St. Gallen, Switzerland*

PACS 61.25.Em – Molecular liquids
PACS 61.05.cm – X-ray reflectometry (surfaces, interfaces, films)
PACS 68.08.-p – Liquid-solid interfaces

Abstract – A silane (tetrakis(trimethylsiloxy)silane) has been confined within a space of a few molecular diameters (9 Å) between two atomically flat opposing mica membranes. The liquid's electron density profile along the confinement direction has been determined by synchrotron X-ray reflectivity for film thicknesses of 8.58 and 11.22 nm. We find the liquid's molecules to be strongly layered at layer distances significantly larger than the effective molecular diameter. The considerable free volume enables the confined liquid to retain its liquid properties.

A liquid which is confined within a slit or pore exhibits properties markedly different from the bulk liquid if it is confined within a space of only a few molecular diameters in size [1]. Such "extreme confinement" imposes a structural ordering to the liquid, which in turn will affect many of the liquid's properties. A considerable part of confined-fluids research has been concerned with measurements of the normal and lateral forces acting between two approaching surfaces in a liquid medium. Typically, oscillatory forces are observed having a periodicity of just below one molecular diameter and an exponential decay of comparable length scale [2–5]. Discrete steps in film thickness are observed, which are commonly interpreted as layering transitions through expulsions of single molecular layers. However, unambiguous electron-density profiles providing proof of such liquid layering have not yet been experimentally determined. More recently, synchrotron X-ray diffraction from various single solid-liquid interfaces and free surfaces revealed structural ordering [6–11]. A recent structural investigation of liquid within a nanometre-sized gap reported thickness quantization between silicon surfaces at externally forced surface separations [12].

Using X-ray reflectivity (XRR) [13] as a function of perpendicular momentum transfer $q_\perp$ we have determined the electron density profile along the confinement direction of the spherical, non-polar liquid tetrakis(trimethylsiloxy)silane (TTMSS) having a molecular diameter of 9.0 Å [8]. The liquid was confined between flat surfaces and the gap width between the surfaces was allowed to equilibrate in the absence of external forces. The confining walls were formed by a pair of (001)-oriented single-crystal surfaces of muscovite mica. The confinement configuration can be regarded as a free-standing single crystal which is interrupted by an ultrathin film of fluid. The advantage of using a crystal lies in its known structure and in its smooth surface provided it is free of atomic steps. The latter is a prerequisite for resolving distinct electron density peaks in the confined liquid. Figure 1 shows a schematic of the confinement geometry and the molecular structure of the mica crystal and TTMSS. Muscovite mica $H_2KAl_3(SiO_4)_3$ is a stack of aluminum silicate sheets separated by sheets of potassium ions. The muscovite (001) planes are easily cleaved due to the absence of covalent bonds between neighboring stacks. The tabled crystal unit cell is monoclinic [14] ($|a| = 5.19$ Å, $|b| = 9.01$ Å and $|c| = 20.05$ Å with $\beta = 95.76°$) and contains c-glide and n-glide planes as symmetry elements. Since the structure is repeated at

(a) E-mail: friso.vanderveen@psi.ch

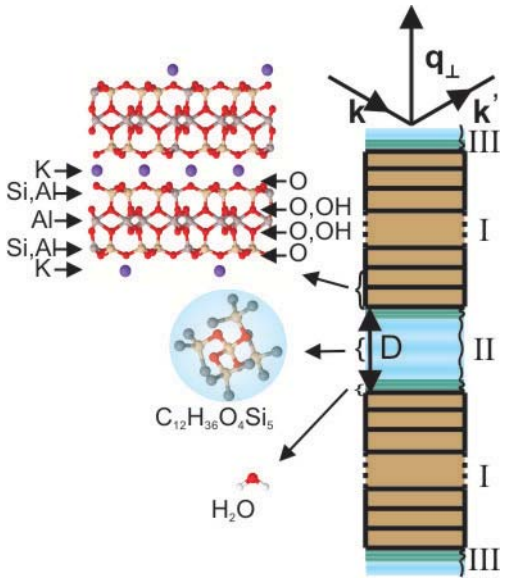

Fig. 1: (Colour on-line) Confinement geometry. Left-hand side: Molecular structures of muscovite mica, tetrakis(trimethylsiloxy)silane (TTMSS) and water. Right-hand side: confinement geometry. The roman numbers indicate the different regions contributing to the X-ray reflectivity: Mica I, liquid in the gap II and the condensed liquid on the outer mica surfaces III. The gap width D is defined as the distance between the surface potassium ions of the opposing mica crystals.

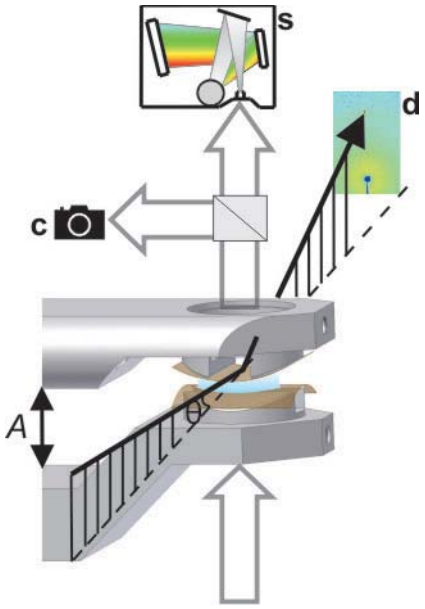

Fig. 2: (Colour on-line) Side view of the confining device in specular X-ray reflection geometry. The piezoelectric actuator A is used to control the gap width. White light is sent through the low-finesse interferometer and analyzed with a spectrometer (s) in order to calculate the gap width with a typical resolution of 20 pm [19–21]. Simultaneously the light is directed into a CCD camera (c) to image the film in real time. The specularly reflected X-rays are analyzed by a PILATUS 100 K detector (d).

$|c|/2$ and $\boldsymbol{q}_\perp$ is parallel to $\boldsymbol{c}$, we take $c' = |c|/2$ as the new height of the unit cell. In this notation, (00ℓ) reflections are zero if the index ℓ is an odd multiple of 1/2. Nevertheless, if any of the symmetry operations is disturbed, such peaks may occur. Since both mica membranes have the same thickness, a symmetric arrangement is obtained. Permanently adsorbed water is found on the inner and outer mica surfaces as is expected from their hydrophilic character [15–17]. Even in a dry environment, an adsorbed water layer is present at the surface planes of potassium ions which we assume to be immobile in our study. A second hydrated water layer is positioned about 1 Å away from the potassium layers. More water layers may condense depending on the relative humidity in the experimental cell [15]. Furthermore, one TTMSS layer condenses on the water-covered outer mica surfaces due to the non-zero vapor pressure.

Our confinement geometry (fig. 2) differs from that of the well-known surface force apparatus (SFA) in that it consists of a crossed pair of curved free-standing mica membranes (fixed to sample holders with large cut-out central regions) instead of the commonly used back-silvered mica membranes glued on solid silica cylinders [18]. This modification allows XRR measurements to be made free of background scattering but makes force measurements impossible (unknown spring constant of mica). The distance between the two mica membranes is adjustable by a micrometre screw and a piezoelectric actuator having 50 pm resolution. Upon fast approach, liquid gets trapped and drains out until a large layered film of typically $300 \times 300\,\mu\text{m}^2$ in size is formed. The stable confined film is essentially free of external forces, which is in contrast to surface force experiments. The mica membranes with liquid medium represent an optical interferometer [19], similar to the one used in the SFA but without solid support and metal mirrors. White light is sent through the interferometer to both measure the gap width and image the lateral extension of the film in real time. The interference spectrum resulting from reflections of the various interfaces is detected by an Ocean Optics (USB 2000) miniature spectrometre. The unknown parameter (gap width or mica thickness) is determined using fast spectral correlation algorithms [19–21]. The mica thickness has to be determined first, in order to obtain the optical reference thickness for subsequent gap width measurements. Note that the zero gap width ($D = 0$) may be shifted by a few ångströms due to an unknown amount of (permanently) bound water to the mica surfaces.

Our method of preparing liquid films under extreme confinement is as follows. After insertion of liquid between the mica sheets, well-chosen cycles of approach and retraction of the mica surfaces generally result in an extremely flat central region containing a film of nanometre thickness and of some hundreds of micrometre in diameter (fig. 3). The motion of the upper mica surface was controlled by an actuator having a range of 25 μm and an approach

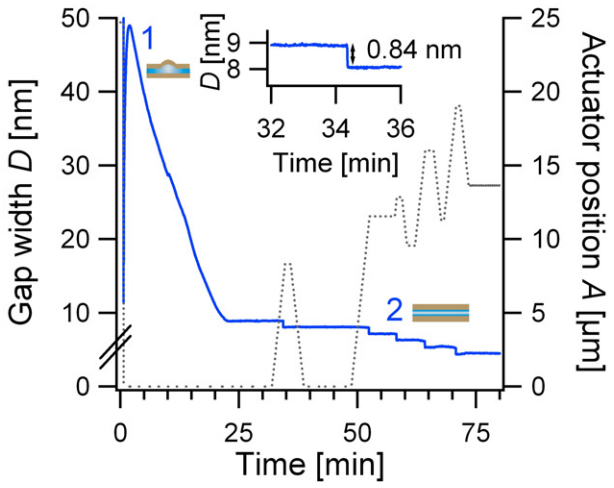

Fig. 3: (Colour on-line) Formation of a confined liquid film (TTMSS) by variation of the actuator position. The gap width D (blue line) measured through white light interference and the actuator's position A (grey dotted line) are plotted against the time. The inset shows the step size of the first layer transition.

speed of ca. 8 μm/s. Decreasing the actuator's position value A reduced the distance D between the mica crystals. The approach mechanism stopped automatically when A reached its zero position. Immediately the two mica surfaces were separated again and liquid got trapped between the mica crystals forming a pocket (region 1 in fig. 3). After ca. twenty minutes the liquid pocket drained out and a flat homogeneous film was formed. Depending on the approach speed large or small separations could be obtained. Moreover, through a sequence of approach and retraction cycles of the membranes we could induce several discrete layer expulsions (region 2 in fig. 3). In order to expel molecular layers from the gap, the value of A was increased. This causes the curvature of the mica and hence the pressure on the film centre to increase. The step size of the layer transitions (see inset region 2 in fig. 3) was usually below the molecular diameter of ~ 9.0 Å [8].

The XRR experiment was performed at the coherent small-angle X-ray scattering beamline (cSAXS) of the Swiss Light Source at the Paul Scherrer Institut. Immediately before the start of the experiment, mica (Spruce Pine Mica, USA) was cleaved into micrometre thin sheets in a laminar flow cabinet to avoid dust. Two pieces from a 5.6 μm thin mica sheet were cut out and glued onto the sample holders. The sample holders were fixed onto the sample stages and surrounded with a cuvette, which was flooded with N_2 to guarantee a dry environment. Relative humidity was recorded next to the sample holders (RHT sensor, Sensirion, Switzerland). This setup was then brought to the measurement station at the beamline. A drop of TTMSS was injected between the mica surfaces using a syringe. A large stable film was obtained using the method described above. Depending on the approach speed of the mica membranes various film thicknesses were obtained. For XRR measurements, we could enlarge the film area at a given thickness by increasing the load without increasing the compression at the centre of the film. A photon wavelength of 0.75 Å (energy 16.5 keV) was selected and focused onto the flat liquid-filled region (focus size H × V of $147 \times 10\,\mu\text{m}^2$). Specularly reflected intensities were measured as a function of perpendicular momentum transfer $q_\perp$ up to $1.4\,\text{Å}^{-1}$ using a single-photon-counting 2D detector (PILATUS 100 K [22], pixel size $172 \times 172\,\mu\text{m}^2$) positioned 0.46 m behind the confinement device. The momentum transfer $q_\perp$ was scanned by tilting the confining device over an angle Θ with respect to the incoming beam direction and recording with the 2D detector the specularly scattered beam at angle 2Θ. At each $q_\perp$ value, the intensity was determined by integration of the scattering intensity at one pixel corresponding to the position of the specular reflection. An intrinsic background arising from diffuse scattering was subtracted. The resulting intensity is the squared modulus of the total structure factor $|F|^2$, multiplied with an angle-dependent factor C which accounts for the Lorentz factor and the illuminated area [23]. F is the sum of the following structure factors: F_I for the stack of unit cells in two mirrored mica crystals at distance D, F_{II} for the liquid in the gap and F_{III} for the condensed liquid on the outer mica surfaces. The total intensity is therefore given by

$$I = C(|F_I|^2 + |F_{II}|^2 + |F_{III}|^2 + 2\,\mathfrak{Re}[F_{II}F_I^*] + 2\,\mathfrak{Re}[F_{III}F_I^*]), \tag{1}$$

where $\mathfrak{Re}$ stands for the real part. The interference term between F_{II} and F_{III} has been dropped since the liquid on the outer mica surfaces and the liquid in the gap scatter incoherently. F_I is calculated from the known crystal structure of mica (assuming crystal termination by on average half a monolayer of potassium), while F_{II} and F_{III} are modeled assuming Gaussian electron density profiles for the liquid layers, where the number of peaks, their height, width and position are to be determined in a fit of various structure models $|F_{\text{calc}}|$ to the measured modulus structure factors $|F_{\text{meas}}|$ using a logarithmic least-squares minimization procedure [24]. The minimized residual Err is given by

$$Err = \sum \frac{[\log(|F_{\text{meas}}|) - \log(|F_{\text{calc}}|)]^2}{[\log(|F_{\text{meas}}|)]^2}. \tag{2}$$

Fits with different number of liquid layers were compared to one another in order to select the best fit. From then on, the number of liquid layers was kept fixed. The number of fitting parameters was further reduced by assuming the confinement arrangement to be symmetric and the TTMSS layers in the gap to have equal electron density and width. The following additional constraints were applied: the liquid was not allowed to penetrate the mica, areal electron densities of the liquid layers were not to exceed the calculated electron density for triangular closest packing (calculated for a molecule diameter of

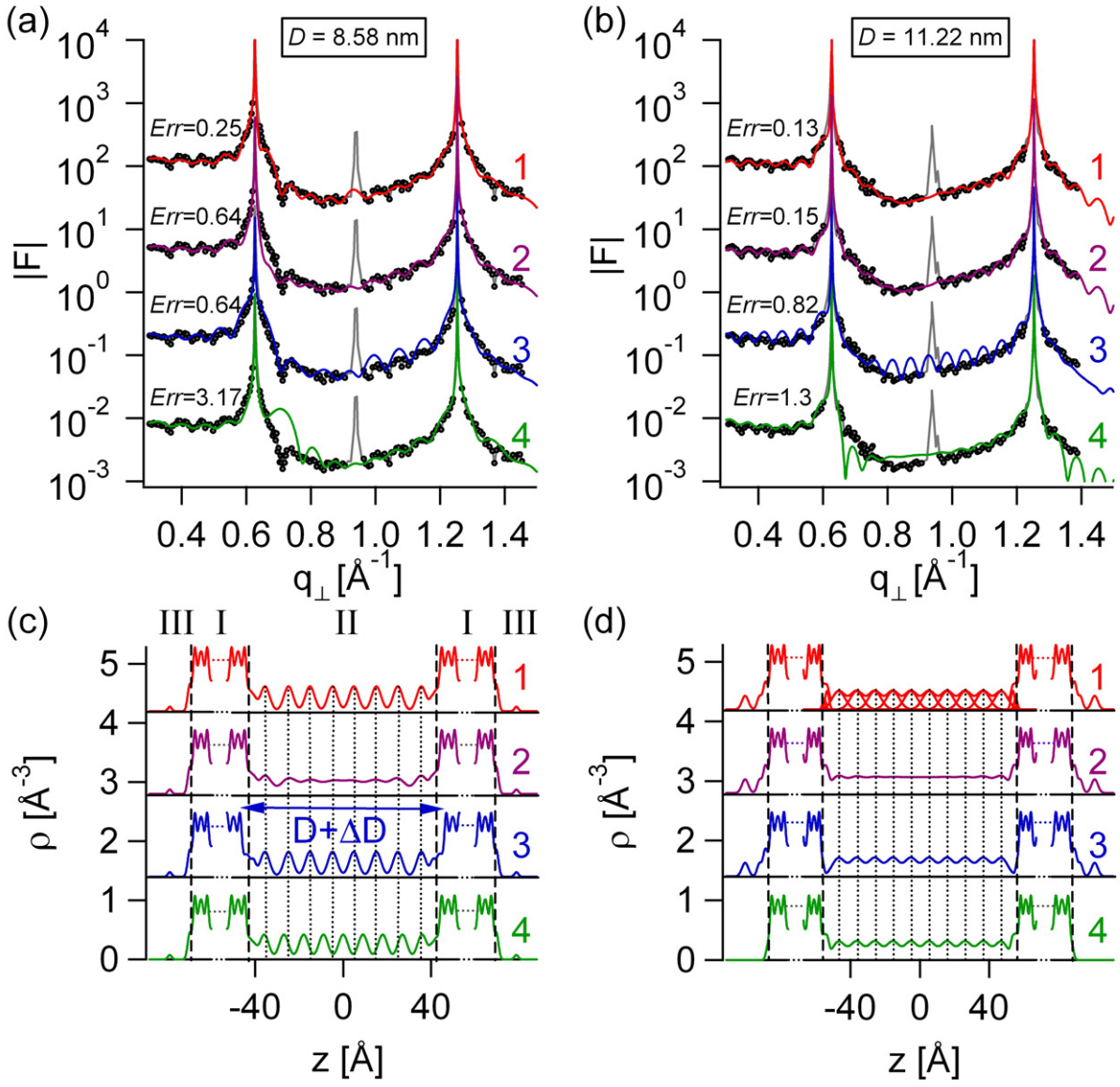

Fig. 4: (Colour on-line) Measured modulus structure factor as a function of momentum transfer $q_\perp$ and calculated structure factors for various model electron density profiles. (a) Measured structure factors for a film thickness of $D = 8.58$ nm are indicated by the grey line (grey dots used for fits). The (001) and (002) mica Bragg peaks are found at 0.63 Å^{-1} and 1.25 Å^{-1}, respectively. The (00 3/2) reflection at 0.9 Å^{-1} results from stacking faults in the mica (not fitted). Curve (1) is the model structure factor providing the best fit to the experimental data. Other calculated structure factors for slightly changed electron density profiles (curves 2–4) have been shifted downwards for better visibility. Structure factors have been calculated for decaying Gaussian peaks (curve 2), a larger film thickness $D = 9.00$ nm (curve 3) and nine layers of TTMSS molecules at distances equal to the molecular diameter (curve 4). (b) Measured structure factors for a film thickness of $D = 11.22$ nm are indicated by the grey line (grey dots used for fits). Curve (1) is the model structure factor providing the best fit to the experimental data. Structure factors have been calculated for the following models: decaying Gaussian peaks (curve 2), missing water peaks on the inner mica surfaces (curve 3) and missing condensed liquid on the outer mica surfaces (curve 4). (c) The corresponding electron density profiles are numbered in accordance to the model structure factors of panel (a). (d) The corresponding electron density profiles are numbered in accordance to the model structure factors of panel (b). Positions of the potassium layers for the best fits are indicated by dashed vertical lines. The TTMSS molecular layer positions for the best fits are indicated by dotted vertical lines. The fit errors are given on the left-hand side of the plots. All electron density profiles have been broadened with the experimental resolution ($\pi/q_{\perp,\max} = 2.2$ Å) [25].

9.0 Å) and the width of the layers was kept to a lower limit of $\sigma = 2$ Å. In all, the least-squares minimization procedure involved the fitting of 20 to 23 free parameters.

Measured and calculated model structure factors are shown in fig. 4(a,b) for two distinct equilibrium film thicknesses ($D = 8.58$ nm and 11.22 nm, determined by XRR).

The XRR data prove to be uniquely sensitive to the liquid film's thickness and structure. Namely, the "interrupted crystal" confinement geometry gives rise to coherent interference effects between the crystal planes at either side of the gap ("Kiessig fringes" [26]), between the crystal planes and the adjacent liquid layers as well as between the liquid layers themselves. The reflectivity curves follow the characteristic shape of a crystal truncation rod [27] (here for mica) but are modulated due to these interference effects. For example, the pronounced broad maximum under the first Bragg peak of mica at $q_\perp = 0.63\,\text{Å}^{-1}$ for both film thicknesses is a signature of the confined liquid being layered with a period about equal to the height of the mica unit cell ($\sim$10 Å). For a film thickness of 8.58 nm, the best fit (curve 1, fig. 4(a)) is obtained for a sequence of nearly equidistant layers at an average separation of 10.12 ± 0.25 Å. This value is higher than the molecular diameter of 9.0 Å (calculated from the bulk number density and cubic packing), which may be attributable to enhanced out-of-plane fluctuations [28].

Under the temporary application of external force on the mica membranes well-defined steps in the film thickness occur. Interpreting such film thickness transitions in terms of the expulsion of a single layer, one would intuitively expect a difference in film thickness equal to the equilibrium layer distance as measured by XRR. Surprisingly, this is not the case; we measure a step size in the film thickness of 8.39 Å (see fig. 3) upon layer expulsion, which is smaller than the equilibrium layer distance by ca 1.7 Å. In general, measured step sizes give only information about the vertical space which is needed to expel a single layer. The layer expulsion process is disordered [29] and therefore one cannot tell which molecules from the confined film are squeezed out. Apparently, the mica membranes slightly relax outward after layer expulsion, with the relaxation being distributed over the confined layer distances.

We deduce from our XRR measurements for a gap width of $D = 8.58$ nm an areal density within the liquids layer plane of $0.011\,\text{Å}^{-2}$, which is lower than for close packing of hard spheres in square or triangular arrangements (0.012 and $0.014\,\text{Å}^{-2}$, respectively). This value for the areal density, combined with a large equilibrium layer distance, results in an average volume density 21% lower than that of bulk liquid and a larger free volume. The TTMSS film therefore appears to have all the structural prerequisites of a liquid, but with a strongly anisotropic thermal disorder [28,30]. At a larger film thickness ($D = 11.22$ nm), the best fit (curve 1, fig. 4(b)) is obtained for a rather diffuse layering as well as a density only 10% lower than that of bulk liquid. The film in the latter case has structural properties much closer to isotropic bulk liquid. We note that this was also the largest film thickness we could experimentally equilibrate as a layered phase (see fig. 3).

The high sensitivity of the CTR modulations to the structural parameters of the confined liquid is illustrated in fig. 4 by the curves 2-4. For example, a model with decaying Gaussian layers (curve 2, fig. 4(c)) results in a less pronounced broad peak under the first mica Bragg peak. A model featuring a 5% larger gap width (curve 3, fig. 4(c)) results in significantly deviating modulations. The assumption of liquid layers at distances equal to the molecular diameter (curve 4, fig. 4(c)) results in a broad maximum peak at a larger momentum transfer than is experimentally observed. The sensitivity to the presence or absence of adsorbed water (curves 3, 4 in fig. 4(d)) is illustrated as well. The calculated modulus structure factor for confined TTMSS in the case of missing water layers on the inner mica surfaces (curve 3) shows that the water layers are damping the fast oscillations resulting from the gap. For missing liquid layers on the outer mica surfaces (curve 4) the overall shape in between the first and second mica Bragg peaks is altered.

We note that there is a limit to the sensitivity of the fitting procedure for electron density profiles that become close to that of bulk liquid. For example, the structure models for smeared layering in curves 1 and 2 of fig. 4(d) result in very similar fits (fig. 4(b)).

In summary, we have determined unambiguously the out-of-plane electron density profile of a molecular liquid in nanometre confinement. Flat confining surfaces at very close distances induced an unexpectedly pronounced layering of the liquid. The large interlayer distances (larger than the molecular diameter) and the low areal densities lead to a considerable free volume enabling the liquid to retain its liquid properties and making layer expulsion still possible.

* * *

The X-ray reflectivity experiment was performed at the cSAXS beamline of the Swiss Light Source, Paul Scherrer Institut, Switzerland. We thank the beamline staff for assistance. This work was supported by the Swiss National Science Foundation.

REFERENCES

[1] Persson B. N. J. and Ballone P., *J. Chem. Phys.*, **112** (2000) 9524.
[2] Mugele F. and Salmeron M., *Phy. Rev. Lett.*, **84** (2000) 5796.
[3] Israelachvili J. N. and Adams G. E., *Nature*, **262** (1976) 773.
[4] Israelachvili J. and Gourdon D., *Science*, **292** (2001) 867.
[5] Christenson H. K. and Bloom C. E., *J. Chem. Phys.*, **86** (1987) 419.
[6] Huisman W. J. and van der Veen J. F., *Surf. Sci.*, **404** (1998) 866.
[7] Reichert H., Klein O., Dosch H., Denk M., Honkimaki V., Lippmann T. and Reiter G., *Nature*, **408** (2000) 839.

[8] Yu C. J., Richter A. G., Kmetko J., Datta A. and Dutta P., *Europhys. Lett.*, **50** (2000) 487.
[9] Yu C. J., Richter A. G., Datta A., Durbin M. K. and Dutta P., *Phys. Rev. Lett.*, **82** (1999) 2326.
[10] Magnussen O. M., Ocko B. M., Regan M. J., Penanen K., Pershan P. S. and Deutsch M., *Phys. Rev. Lett.*, **74** (1995) 4444.
[11] Tweet D. J., Holyst R., Swanson B. D., Stragier H. and Sorensen L. B., *Phys. Rev. Lett.*, **65** (1990) 2157.
[12] Seeck O. H., Kim H., Lee D. R., Shu D., Kaendler I. D., Basu J. K. and Sinha S. K., *Europhys. Lett.*, **60** (2002) 376.
[13] Als-Nielsen J. and McMorrow D., *Elements of Modern X-ray Physics* (John Wiley and Sons, New York) 2001.
[14] Güven N., *Z. Kristallogr.*, **134** (1971) 196.
[15] Malani A. and Ayappa K. G., *J. Phys. Chem. B*, **113** (2009) 1058.
[16] Christenson H. K., *J. Phys. Chem.*, **97** (1993) 12034.
[17] Balmer T. E., Christenson H. K., Spencer N. D. and Heuberger M., *Langmuir*, **24** (2008) 1566.
[18] Israelachvili J. N. and McGuiggan P. M., *J. Mater. Res.*, **5** (1990) 2223.
[19] Born M. and Wolf E., *Principles of Optics* (Pergamon Press, Oxford) 1980.
[20] Clarkson M. T., *J. Phys. D: Appl. Phys.*, **22** (1989) 475.
[21] Heuberger M., *Rev. Sci. Instrum.*, **72** (2001) 1700.
[22] Kraft P., Bergamaschi A., Broennimann C., Dinapoli R., Eikenberry E. F., Henrich B., Johnson I., Mozzanica A., Schleputz C. M., Willmott P. R. and Schmitt B., *J. Synchrotron Radiat.*, **16** (2009) 368.
[23] Torrelles X. and Rius J., *J. Appl. Crystallogr.*, **37** (2004) 395.
[24] Hirano T., Usami K., Ueda K. and Hoshiya H., *J. Synchrotron Radiat.*, **5** (1998) 969.
[25] Fenter P. A., in *Applications of Synchrotron Radiation in Low-Temperature Geochemistry and Environmental Science*, edited by Fenter P., Rivers M., Sturchio N. and Sutton S., *Rev. Mineral. Geochem.*, **49** (2002) 149.
[26] Kiessig H., *Ann. Phys. (Leipzig)*, **10** (1931) 769.
[27] Robinson I. K., *Phys. Rev. B*, **33** (1986) 3830.
[28] Mittal J., Truskett T. M., Errington J. R. and Hummer G., *Phys. Rev. Lett.*, **100** (2008) 145901.
[29] Becker T. and Mugele F., *Phys. Rev. Lett.*, **91** (2003) 166104.
[30] Snook I. K. and Henderson D., *J. Chem. Phys.*, **68** (1978) 2134.